



**HAL**  
open science

## Top-hat beam output of a single-mode microstructured optical fiber: Impact of core index depression

Constance Valentin, Pierre Calvet, Yves Quiquempois, Géraud Bouwmans, Laurent Bigot, Quentin Coulombier, Marc Douay, Karen Delplace, Arnaud Mussot, Emmanuel Hugonnot

### ► To cite this version:

Constance Valentin, Pierre Calvet, Yves Quiquempois, Géraud Bouwmans, Laurent Bigot, et al.. Top-hat beam output of a single-mode microstructured optical fiber: Impact of core index depression. Optics Express, 2013, 21 (20), pp.23250. 10.1364/OE.21.023250 . hal-00903415

**HAL Id: hal-00903415**

**<https://hal.science/hal-00903415>**

Submitted on 12 Nov 2013

**HAL** is a multi-disciplinary open access archive for the deposit and dissemination of scientific research documents, whether they are published or not. The documents may come from teaching and research institutions in France or abroad, or from public or private research centers.

L'archive ouverte pluridisciplinaire **HAL**, est destinée au dépôt et à la diffusion de documents scientifiques de niveau recherche, publiés ou non, émanant des établissements d'enseignement et de recherche français ou étrangers, des laboratoires publics ou privés.

# Top-hat beam output of a single-mode microstructured optical fiber: Impact of core index depression

Constance Valentin,<sup>1,\*</sup> Pierre Calvet,<sup>1,2</sup> Yves Quiquempois,<sup>1</sup> Géraud Bouwmans,<sup>1</sup> Laurent Bigot,<sup>1</sup> Quentin Coulombier,<sup>1</sup> Marc Douay,<sup>1</sup> Karen Delplace,<sup>1</sup> Arnaud Mussot,<sup>1</sup> and Emmanuel Hugonnot<sup>2</sup>

<sup>1</sup>Laboratoire de Physique des Lasers, Atomes et Molécules, UMR 8523, Institut de Recherche sur les Composants logiciels et matériels pour l'Information et la Communication Avancée, USR CNRS 3380, 50 Avenue Halley, F-59658 Villeneuve d'Ascq Cedex, France

<sup>2</sup>Commissariat à l'Energie Atomique et aux Énergies Alternatives, Centre d'Études Scientifiques et Techniques d'Aquitaine, 15 avenue des Sablières, CS 60001, 33116 Le Barp Cedex, France  
[constance.valentin@univ-lille1.fr](mailto:constance.valentin@univ-lille1.fr)

**Abstract:** A new strategy to obtain a single-mode fiber with a flattened intensity profile distribution is presented. It is based on the use of an OVD-made high index ring deposited on a silica rod having a refractive index slightly lower than the silica used for the microstructured cladding. Using this strategy, we realized the first single-mode fiber with a quasi-perfect top-hat intensity profile around 1  $\mu\text{m}$ . Numerical studies clearly demonstrate the advantage of using a core index depression to insure the single-mode operation of the fiber at the working wavelength.

©2013 Optical Society of America

**OCIS codes:** (060.4005) Microstructured fibers; (060.2270) Fiber characterization; (060.2280) Fiber design and fabrication; (060.2400) Fiber properties.

---

## References and links

1. D. J. Richardson, J. Nilsson, and W. A. Clarkson, "High power fiber lasers: current status and future perspectives," *J. Opt. Soc. Am.* **27**(11), B63–B92 (2010).
2. L. Lago, D. Bigourd, A. Mussot, M. Douay, and E. Hugonnot, "High-energy temporally shaped nanosecond-pulse master-oscillator power amplifier based on ytterbium-doped single-mode microstructured flexible fiber," *Opt. Lett.* **36**(5), 734–736 (2011).
3. F. M. Dickey and S. C. Holswade, *Laser Beam Shaping, Theory and Techniques* (Marcel Dekker Inc, 2000).
4. Y. Matsuura, M. Miyagi, A. German, L. Nagli, and A. Katzir, "Silver-halide fiber tip as a beam homogenizer for infrared hollow waveguides," *Opt. Lett.* **22**(17), 1308–1310 (1997).
5. Y. Matsuura, D. Akiyama, and M. Miyagi, "Beam homogenizer for hollow-fiber delivery system of excimer laser light," *Appl. Opt.* **42**(18), 3505–3508 (2003).
6. J. R. Hayes, J. C. Flanagan, T. M. Monro, D. J. Richardson, P. Grunewald, and R. Allott, "Square core jacketed air-clad fiber," *Opt. Express* **14**(22), 10345–10350 (2006).
7. A. K. Ghatak, I. C. Goyal, and R. Jindal, "Design of waveguide refractive index profile to obtain flat modal field," *Proc. SPIE* **3666**, 40–44 (1999).
8. J. W. Dawson, R. Beach, I. Jovanovic, B. Wattellier, Z. M. Liao, S. A. Payne, and C. P. J. Barty, "Large flattened mode optical fiber for reduction of non-linear effects in optical fiber lasers," *Proc. SPIE* **5335**, 132–139 (2004).
9. X. Lu, Q. Zhou, J. Qiu, C. Zhu, and D. Fan, "Design guidelines and characteristics of beam-shaping microstructure optical fibers," *Opt. Commun.* **259**(2), 636–639 (2006).
10. C. Wang, F. Zhang, Y. Lu, C. Liu, R. Geng, and T. Ning, "Photonic crystal fiber with a flattened fundamental mode for the fiber lasers," *Opt. Commun.* **282**(11), 2232–2235 (2009).
11. C. Wang, F. Zhang, Y. Lu, C. Liu, R. Geng, T. Ning, and S. Jian, "Single mode operations in the large flattened mode optical fiber lasers and amplifiers," *J. Opt. A, Pure Appl. Opt.* **11**(6), 065402 (2009).
12. J. K. Sahu, S. Yoo, A. J. Boyland, A. S. Webb, M. Kalita, J. N. Maran, Y. Jeong, J. Nilsson, W. A. Clarkson, and D. N. Payne, "Fiber design for high-power fiber lasers," *Proc. SPIE* **7195**, 71950I, 71950I-13 (2009).
13. N. N. Elkin, A. P. Napartovich, V. N. Troshchieva, and D. V. Vysotsky, "Modelling of large flattened mode area fiber lasers," *Laser Phys.* **20**(2), 304–310 (2010).
14. J. W. Dawson, Z. M. Liao, I. Jovanovic, B. Wattellier, R. Beach, S. A. Payne, and C. P. J. Barty, "Large flattened mode optical fiber for high output energy pulsed fiber lasers," in *Proceedings of CLEO 2003*, paper CWD5, (2003).

15. C. Valentin, Y. Quiquempois, G. Bouwmans, L. Bigot, M. Douay, A. Mussot, L. Lago, P. Calvet, and E. Hugonnot, "Flattened fundamental mode in microstructured fibers: design, realization and characterization," *Proc. SPIE* **8426**, 84260J, 84260J-5 (2012).
16. P. Calvet, C. Valentin, Y. Quiquempois, G. Bouwmans, L. Bigot, M. Douay, A. Mussot, and E. Hugonnot, "Top-hat beam output from a large mode area microstructured fiber for beam delivery," *Proc. SPIE* **8433**, 84330K, 84330K-7 (2012).
17. J. Limpert, N. Deguil-Robin, I. Manek-Höninger, F. Salin, F. Röser, A. Liem, T. Schreiber, S. Nolte, H. Zellmer, A. Tünnermann, J. Broeng, A. Petersson, and C. Jakobsen, "High-power rod-type photonic crystal fiber laser," *Opt. Express* **13**(4), 1055–1058 (2005).
18. K. Saitoh, Y. Tsuchida, M. Koshiba, and N. A. Mortensen, "Endlessly single-mode holey fibers: the influence of core design," *Opt. Express* **13**(26), 10833–10839 (2005).
19. P. S. J. Russell, "Photonic-crystal fibers," *J. Lightwave Technol.* **24**(12), 4729–4749 (2006).
20. F. Hanawa, Y. Hibino, M. Shimizu, H. Suda, and M. Horiguchi, "Influences of the drawing conditions on optical characteristics in undoped-silica-core single-mode fibers," *Opt. Lett.* **12**(8), 617–618 (1987).
21. J. W. Nicholson, A. D. Yablon, S. Ramachandran, and S. Ghalimi, "Spatially and spectrally resolved imaging of modal content in large-mode-area fibers," *Opt. Express* **16**(10), 7233–7243 (2008).
22. D. M. Nguyen, T. N. Nguyen, S. Blin, M. Thual, and T. Chartier, "Scalar product technique in modal decomposition for multimode fibers," *Proc. SPIE* **7717**, 77170V, 77170V-10 (2010).
23. Y. O. Agha, F. Zolla, A. Nicolet, and S. Guenneau, "On the use of PML for the computation of leaky modes: an application to microstructured optical fibres," *Int. J. Computation Math. Elec. Electron. Engineer.* **27**(1), 95–109 (2008).
24. G. J. Pearce, T. D. Hedley, and D. M. Bird, "Adaptive curvilinear coordinates in a plane-wave solution of Maxwell's equations in photonic crystals," *Phys. Rev. B* **71**(19), 195108 (2005).
25. W. Boutu, T. Auguste, O. Boyko, I. Sola, P. Balcou, L. Binazon, O. Gobert, H. Merdji, C. Valentin, E. Constant, E. Mével, and B. Carré, "High-order-harmonic generation in gas with a flat-top laser beam," *Phys. Rev. A* **84**(6), 063406 (2011).
26. E. Constant, A. Dubrouil, O. Hort, S. Petit, D. Descamps, and E. Mével, "Spatial shaping of intense femtosecond beams for the generation of high-energy attosecond pulses," *J. Phys. At. Mol. Opt. Phys.* **45**(7), 074018 (2012).
27. A. Dubrouil, Y. Mairesse, B. Fabre, D. Descamps, S. Petit, E. Mével, and E. Constant, "Controlling high harmonics generation by spatial shaping of high-energy femtosecond beam," *Opt. Lett.* **36**(13), 2486–2488 (2011).

---

## 1. Introduction

Fiber technology has a great potential to improve the compactness, stability and versatility of laser systems, without any free-space alignment [1]. Recent progresses in fiber laser technologies have proven their capability to deliver high-power pulses suitable for industrial needs (laser marking, welding, cutting, drilling and heat treatment), for laser-biological tissues interactions inside the body, for fundamental studies in laser-matter interaction processes or for seeding large-scale laser facilities like Laser MegaJoule (LMJ) [2]. Currently, the intensity profile at the output of a standard single-mode fiber exhibits a Gaussian-like structure. As a result, the intensity deposited on the target (material, biological tissue, etc) is not uniform and the treatment leads to irregularities. Top-hat intensity patterns are then more suited for such applications. The simplest way to achieve such a shaping is to use beam aperturing at the fiber output but at the expense of very high losses. Other laser beam shaping techniques such as field mapping or use of beam integrators are very interesting because they imply no loss [3]. However, the alignment of field mapping setups is very tricky and beam integrators deliver poorly coherent beams in the spatial domain, which is detrimental for most applications. To avoid the use of complex beam shaping optics, an elegant and efficient solution is to achieve an all-fiber system that directly delivers a 'top-hat' beam profile. Highly multimode fibers represent the usual way to homogenize the field distribution and flat-top beam profiles with circular or square shape have been already demonstrated [4–6]. However, such fibers exhibit very low depth of focus and spatial incoherence (i.e. random phase profiles). Accordingly, a very interesting and reliable way to obtain a flat-top delivered beam with large depth of focus is to use an optical fiber with a tailored index profile that flattens the intensity distribution of the fundamental mode [7]. Note that such a fiber structure also presents the great advantage to increase the threshold for nonlinear effects, as compared to a structure having the same mode field diameter but delivering a Gaussian-like shape mode [8].

In the past, several fiber designs (including more recently microstructured optical fibers) [9–13] have been proposed to obtain a flattened fundamental mode but most of these studies were only numerical and fiber designs were usually slightly multimode at the operating

wavelength, which is detrimental for many applications. Only few papers report on experimental results [8, 14]. However, even if the beam profile was indeed more flattened than the usual Gaussian-like profile, it was still far from the ideal top-hat profile because of practical fabrication issues leading to a deviation from the ideal refractive index profile. This is only very recently that we reported preliminary experimental results on fibers that deliver a fundamental mode with a real flattened profile [15, 16].

In this paper, we present in details a new strategy to obtain intrinsically single-mode fibers at the operating wavelength with very good intensity flatness. In particular, we demonstrate through numerical simulations that core's higher order modes can be made extremely lossy by using a refractive index-depressed core compare to the silica used in the microstructured cladding. The single-mode behavior of our flattened mode fiber is demonstrated for the first time through meticulous experimental characterizations. The key processes to obtain such notable results are also detailed.

The paper is organized as follows: after recalling the operating principle of flattened mode fiber, we detail in section 2 our strategy to realize a single-mode fiber with a quasi-perfect top hat profile and its realization. Its optical properties are described in section 3. Numerical studies based on the geometrical parameters of the fabricated fiber are presented in section 4 and demonstrate the advantage of using index-depressed core. Finally, a conclusion and applications are given in section 5.

## 2. Fiber design and realization

### 2.1. Operating principle

Figure 1(a) represents the basic index profile that enables to get a flattened fundamental mode. It is based on three ingredients, namely a thin high index ring (1) that is added between the core (2) and the cladding (3) of a conventional step index fiber. The operating principle of such structure is illustrated on Fig. 2 and can be simply explained as follows. At sufficiently short wavelengths, the fundamental mode of the fiber is well confined in the high index ring with an exponential-like decrease (evanescent fields) in both cladding and core media: the effective index of the core mode is close to the refractive index of the ring. Here, the intensity decrease is faster in the cladding because of its higher refractive index difference with the mode effective index. As wavelength increases, the fundamental mode spreads more and more out of the high index ring and its effective index decreases (see Fig. 2). At a specific wavelength, the electrical field is no more evanescent in the core (while being still evanescent in the cladding): the effective index becomes equal to the refractive index of the core. This is at that particular wavelength that a core mode with a flat profile can be obtained and it corresponds to the cut-off wavelength of the ring mode. For longer wavelengths, the effective index of the guided mode keeps decreasing and its intensity starts peaking at the core center. By further increasing the wavelength, the thin ring structure is no more perceived by the light so that the mode is then very similar to the fundamental mode of a standard fiber and presents a Gaussian-like intensity profile (see Fig. 2).

From the above explanation, one can understand that the wavelength at which the flat mode is obtained depends mostly on the high index ring size and on its refractive index difference with the core. On the other side, the number of modes supported by the structure is mainly driven by the core size and its refractive index difference with the cladding (as in conventional step index fibers).

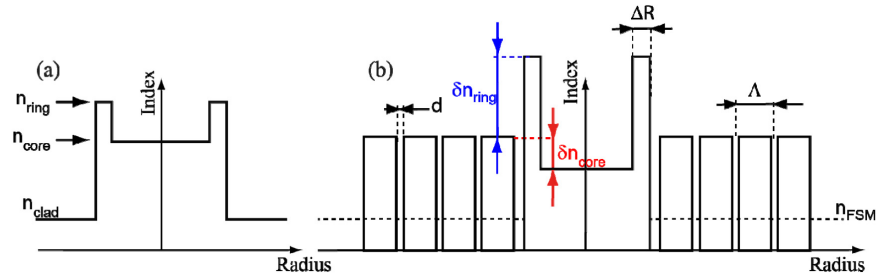


Fig. 1. Index profiles for step-index (a) and microstructured (b) fiber to obtain a flat top intensity profiles at the fiber output.  $n_{ring}$ ,  $n_{core}$  and  $n_{clad}/n_{FSM}$  correspond to the refractive indices of the ring, the core and the cladding, respectively. For the microstructured fiber, we denote  $\delta n_{core}$  and  $\delta n_{ring}$  the core and the ring index contrast with respect to the silica used in the cladding, respectively.  $\Delta R$  is the ring thickness,  $\Lambda$  the pitch of the cladding and  $d$  the diameter of the air holes.

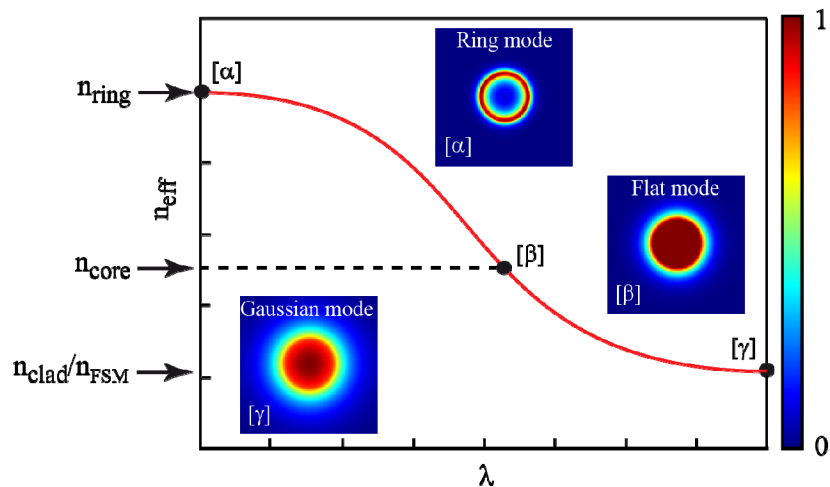


Fig. 2. Schematic evolution (without considering material dispersion) of the fundamental mode effective index for the index profile of Fig. 1(a). The insets show typical intensity profiles at short ( $\alpha$ ) and long ( $\gamma$ ) wavelengths compared to the cut-off wavelength of the fundamental ring mode ( $\beta$ ).

## 2.2 Strategy to get large mode and intrinsically single-mode fiber with a flattened mode

Our strategy to obtain large mode area single-mode fibers with a flattened mode profile is based on (i) using an air/silica cladding, (ii) fabricating the high index ring by Outside Vapor Deposition (OVD) process and (iii) using a core material with a refractive index slightly lower than that of the silica used in the cladding (see Fig. 1(b)). The reasons and more details on this novel strategy are given hereafter:

(i) First of all, an air-silica cladding (as Ref. 9-11) allows refractive index to be very close to silica, which would be very tricky to obtain with a solid homogeneous cladding. Moreover, it also enables to finely adjust the contrast,  $\Delta n$ , between cladding and core indices by adjusting the parameter  $d/\Lambda$  during the final drawing process with fine control of the size of the air holes. Both of these properties obviously represent key ingredients to obtain a single-mode large effective area optical fiber. To do so, we opted for a microstructured fiber with a 7-cell defect core as it permits to obtain a large core diameter without requiring a too large pitch of the periodical structure [17]. Note, however, that the ratio between the hole diameter,  $d$ , and the pitch,  $\Lambda$ , has to be kept small to insure single-mode guidance (below 0.046 if the endlessly single-mode regime is targeted [18]).

(ii) Realizing the high index ring by the OVD process makes it possible to ensure a very good control of its opto-geometrical parameters (thickness, refractive index), decoupled from the synthesis of the glass rod that will be used as core: the composition and refractive index of this rod can hence be adjusted independently of that of the high-index ring. The final overcladded rod is compatible with Stack and Draw technique processing and can be used as the core of a microstructured fiber whose cladding geometry can also be adjusted freely: properties of the core, high index ring and micro-structured cladding are hence precisely and separately adjusted at different steps of the process.

(iii) Using a central rod with a slightly depressed refractive index enables us to decrease the effective indices of the core modes, so that only the fundamental core mode has low confinement loss. Indeed all high order modes with effective index lower than (or close enough to) the cladding refractive index  $n_{\text{FSM}}$  are not (or only very weakly) confined into the core region. Note that the number of core modes could also be reduced by increasing the cladding refractive index but this would require an accurate control of small values of  $d/\Lambda$  ( $\sim 0.03$ ), which is very challenging in terms of fabrication. Thereby, a decrease of the refractive index of the core enables to reach a single-mode behavior with a smaller cladding refractive index and thus a larger  $d/\Lambda$  which greatly facilitates the fabrication process.

### 2.3. Fiber fabrication

Figure 3(a) shows a Scanning Electron Microscope (SEM) image of a typical fiber (called hereafter Fiber A) fabricated using the Stack and Draw process [19]. First a hexagonal stack of 127 silica capillaries (6 rings) drawn from a high quality pure silica tube (Heraeus F300) has been realized. In this stack, the 7 central capillaries were replaced by a solid capillary containing the high index ring and drawn from a solid rod. The high index ring was realized by OVD – see description below – and is clearly visible on the SEM picture. In order to get a cladding with small enough  $d/\Lambda$  (typically  $< 0.2$ ), additional capillaries, also drawn from a F300 Heraeus tube, were inserted in each of the previous capillaries. The outside ring of capillaries was then partially removed to enable the stack to be inserted into a circular jacketing tube. Note that a F320 Heraeus tube (F-doped silica) was used as a jacketing tube: it presents a refractive index difference of  $-1.2 \times 10^{-3}$  as compared to the F300 material. The use of a low index outer cladding was chosen in order to reduce easily the confinement loss without the need of extra air holes rings. These different operations lead to a preform presenting 4 complete rings of air holes and a partial 5th ring featuring 18 extra holes. This stack of 25 mm Outside Diameter (OD) was then drawn into 4 mm canes that were jacketed in 8 mm OD tube before the final drawing process.

As mentioned before, the OVD process has been used to realize the high index ring around the central core. More precisely twelve layers of germanium-doped (Ge-doped) silica have been deposited and sintered on a commercial silica rod of 18 mm of diameter. Note that two pure silica layers were deposited on the Ge-doped ones so as to limit the germanium oxide depletion of the outer Ge-doped layers, due to diffusion during the different heating and drawing process. Finally, this rod was drawn into a  $\sim 4$  mm rod used as the central core of the stack. Because of its nanometric size, no direct measurement of the ring index profile was possible at the fiber stage. The refractive index profile of the high index ring was then deduced from the germanium concentration profile obtained by Electron Probe Micro-Analysis (EPMA) measurements done on the 4 mm rod (see Fig. 3(b)). It has been evaluated to  $+ 5 \times 10^{-3}$  as compared to the refractive index of the F300 tubes used for the cladding. The thickness of the ring,  $\Delta R$ , in the final fiber was estimated by assuming a homothetic transformation of the transversal dimensions measured on the 4 mm rod. Finally, as mentioned in section 2.2, our aim was to use a silica core presenting a refractive index slightly lower than that of the silica used in the cladding air-silica. For this reason a LWQ100 rod from Heraeus was used as core material. Its refractive index difference with F300 has been estimated to about  $-0.4 \times 10^{-3}$  at 1550 nm, by home-made measurements. However, it has to be pointed out that uncertainty on this value is quite large (accuracy of the measurement is  $\pm$

$0.2 \times 10^{-3}$  for conventional single-mode preform, which is far from being the case here). Moreover this refractive index difference could also be significantly modified during the drawing process [20]. Thus, at this stage of discussion, the refractive index difference between the silica used for the core and the one used for the air-silica cladding (i.e.  $\delta n_{core}$  on Fig. 1(b)) is supposed to be between 0 and  $-1 \times 10^{-3}$  in the final fiber at the operating wavelength.

By simply adjusting the pitch  $A$  and the ratio  $d/A$  during final drawing, it has been possible to realize a single-mode fiber that presents a flattened fundamental mode around  $1 \mu\text{m}$  with relatively low losses. The detailed characterization of this particular fiber (Fiber A) is presented in the next section.

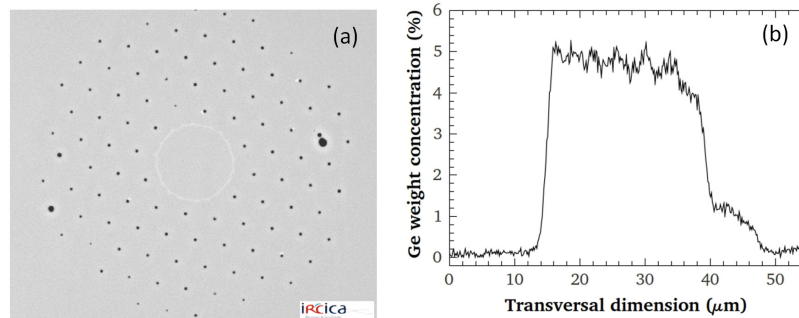


Fig. 3. (a) Scanning electron micrograph image of Fiber A. The dark regions correspond to the air holes while the high index ring is the bright gray central ring. (b) Radial profile of germanium concentration of the high-index ring measured by EPMA.

From the SEM image, we have measured a pitch,  $A$ , of  $5.42 \mu\text{m}$ , a ratio,  $d/A$ , of 0.12, a low index core radius of  $6.74 \mu\text{m}$  and we have estimated a ring thickness of 260 nm from homothetic transformation. As mentioned before, the refractive index of this ring is estimated by calibration from the germanium concentration to be  $+5 \cdot 10^{-3}$  higher than the silica used to realize the cladding.

### 3. Optical characterizations

#### 3.1 Output intensity profile and single-mode behavior

A first characterization has been performed by injected a supercontinuum source in a 2 m-long piece of the fiber described above. The near field was imaged on an Infrared camera at different wavelengths using bandpass filters ( $\sim 10 \text{ nm}$  FWHM), placed before the injection lens. Typical results are depicted in Fig. 4. As expected, one can clearly see the transformation of the fundamental mode from a donut mode at  $650 \text{ nm}$  to a Gaussian-like mode at  $1650 \text{ nm}$  (see section 2.1 and Fig. 2). A flattened mode is obtained in the  $950\text{--}1150 \text{ nm}$  wavelength range with a nearly perfect flat top intensity profile at  $1050 \text{ nm}$ .

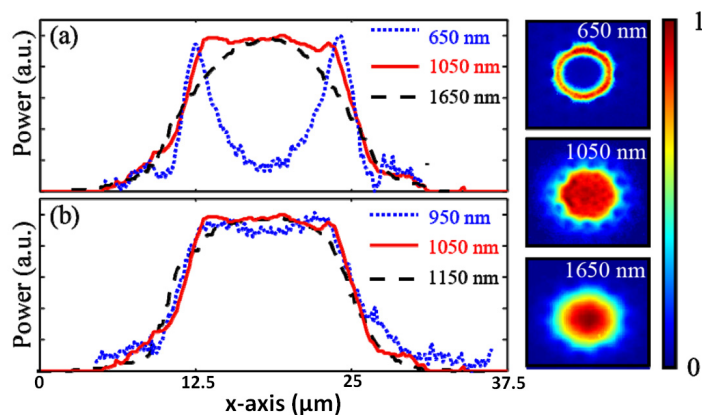


Fig. 4. Experimental transverse profiles of fundamental mode near field images at different wavelengths from 650 to 1650 nm (a) and from 950 to 1150 nm (b).

The effective area at 1.05  $\mu\text{m}$  has been estimated from experimental image to 320  $\mu\text{m}^2$  corresponding to a mode field diameter of about 20  $\mu\text{m}$ . It is worth noting that whatever the injection conditions with this setup, the same intensity distribution was recorded at the output of the fiber (only the coupling efficiency was modified) even for fiber lengths as short as 27 cm. This behavior is a first indication that Fiber A does not support any Higher Order Modes (HOM). This observation being only qualitative, the modal content of the fiber core has been measured by a spatially and a spectrally resolved imaging technique, the so-called  $S^2$  technique first reported by Nicholson *et al.* [21].

Following the experimental setup described by N'Gyuen *et al.*, we used a tunable narrow-bandwidth laser and an Infrared camera to perform the  $S^2$  measurement [22]. For each camera pixel, an interference spectrum originating from the beating between guided modes can be recorded. For each HOM supported by the fiber a peak appears in the Fourier transforms of these spectra. The numerical treatment of these Fourier transforms gives the intensity profiles of the modes supported by the fiber, their relative power and their relative group delay. To ensure the validity of our  $S^2$  measurement, we first characterized a slightly different fiber, called hereafter Fiber B. Its pitch (6.88  $\mu\text{m}$ ) and  $d/\Lambda$  ratio (0.19) were higher than those of Fiber A, which makes this fiber indeed multimode. Both fibers have been designed to support a fundamental mode with a top-hat shape around 1.05  $\mu\text{m}$  and are 5.5 m long. In Fig. 5(a) we plot the summation over the pixels of all Fourier transforms for Fiber B (blue line) and for Fiber A (solid red and black lines). Besides continuous component peak, Fiber B exhibits a peak corresponding to interferences between the fundamental mode and the first HOM for a 9.5 ps group delay (corresponding to a group index difference  $\delta n_g$  of  $5.23 \times 10^{-4}$ ). The reconstructed images of the fundamental and first HOM intensity distribution as well as the group delay are in good agreement with the ones obtained directly through numerical calculations (see Fig. 5(b)).

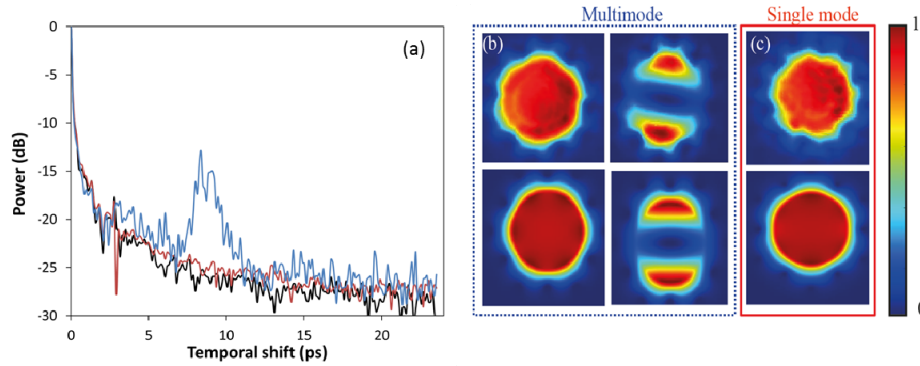


Fig. 5. Results of the  $S^2$  measurements around  $1.05 \mu\text{m}$ : (a) Sum of all Fourier transforms over all the pixels for Fiber B (blue line) and Fiber A. For Fiber A, centered injection has been tested (black line) together with an off-centered one ( $15 \mu\text{m}$  offset, red line). Fundamental and first higher order modes intensity distributions for Fiber B (b) and Fiber A (c) (top: image retrieved by  $S^2$  algorithm using experimental data, bottom: mode profiles obtained numerically (see section 4)).

Conversely to Fiber B, no peak was detected for Fiber A (Fig. 5(a)) even when a  $15 \mu\text{m}$  lateral offset was applied on injection (red line). The reconstructed image of the fundamental mode shown on Fig. 5(c) is very similar to the one observed directly. We can emphasize that several  $S^2$  measurements have been performed with different input-coupling conditions and different bend radii. Whatever these parameters, no HOM interference peak has been detected. It is thus clear that Fiber A can be considered as a single-mode fiber with a flat-top intensity profile at wavelengths around  $1.05 \mu\text{m}$ .

### 3.2 Losses characterization

In order to characterize the optical losses, we first performed a cut-back measurement on a piece of Fiber A kept as straight as possible. In a second time, we measured the extra losses induced by bending the fiber. For the cut-back measurement, a  $20 \text{ mW}$  narrow-bandwidth continuous-wave laser at  $1.053 \mu\text{m}$  was launched into a  $3 \text{ m}$ -long piece of Fiber A using an aspherical lens ( $6.2 \text{ mm}$  focal length and  $0.4$  numerical aperture). The fiber attenuation deduced from these measurements is  $0.23 \text{ dB/m}$  (Fig. 6(a)). This relatively high value could probably be reduced by increasing the size of the cladding (see the rather high confinement loss values obtained in section 4). Nevertheless, for most of the applications requiring a flattened mode, one need only few meters of fiber so our present experimental loss value is not a limitation. Furthermore, it is important to note that the coupling losses are only about  $0.6 \text{ dB}$  when splicing Fiber A to standard step-index fiber with  $15 \mu\text{m}$  core diameter. It represents an important advantage to implement these fibers in all-fiber setups.

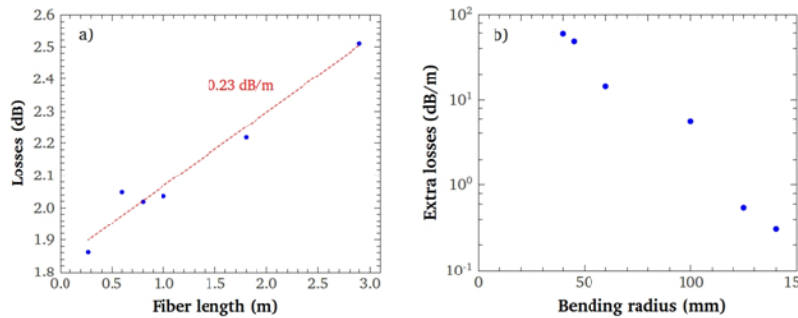


Fig. 6. (a) Cut-back measurements: experimental data (blue filled circles), linear fit (red dashed line). (b) Extra losses induced by bending the fiber at  $1.05 \mu\text{m}$ .

The evolution of the extra losses at 1050 nm induced by bending the fiber is shown in Fig. 6(b). These results are deduced from the measurement of the output power of a 1.7 m long fiber for several bending radii, the output power reference being the one obtained for the straight fiber. Bending this fiber with radius of curvature lower than 10 cm will lead to significant extra-losses ( $> 5$  dB/m). As in large mode area fibers, leakage of the mode is easily achieved by bending the fiber, because of the small effective indices difference between core and cladding modes.

During all these measurements, we have checked on a CCD camera that the flat-top fundamental mode is not coupled to any HOM but only to cladding modes, confirming again the single-mode property of Fiber A.

#### 4. Numerical study of the impact of core index depression

To prove that decreasing the core refractive index is indeed a key point to explain the experimental results above-described, we present hereafter a numerical study of the impact of the core index depression on the fiber properties. To achieve this goal, we have performed numerical simulations using a finite element method (COMSOL Multiphysics). A perfectly matched layer (PML) [23] has been added to the outer boundaries of the computational domain to avoid reflections of electromagnetic fields and to calculate optical losses of the core modes. The transverse structure used for the numerical calculation is based on the opto-geometrical parameters of Fiber A except for the Ge-doped ring boundaries that have been assumed to be perfect circles. Indeed, preliminary calculations have shown that a deformed ring structure does not lead to a significant modification of the guided mode pattern provided that the thickness of the ring is kept constant, which is the case here. The air/silica cladding is similar to the experimental one with 5 rings of air-holes, the 5th one not being entire. The pitch was fixed to  $5.42 \mu\text{m}$  and  $d/\Lambda$  to 0.12. The down-doped layer due to the F320 jacketing tube (cf. section 2.3) was also taken into account by adding on the outside of this air silica cladding a ring of  $9.9 \mu\text{m}$  with a refractive index difference of  $-1.2 \times 10^{-3}$  compare to the silica index used in the cladding. The external diameter of the high index ring and its refractive index contrast,  $\delta n_{opt}$ , were set to  $7 \mu\text{m}$  and  $+ 5 \times 10^{-3}$  respectively. The refractive index depression of the core,  $\delta n_{core}$ , was varied from 0 to  $-9 \times 10^{-4}$ . For each value of  $\delta n_{core}$ , we had to adjust the ring thickness  $\Delta R$  to obtain a flat-top profile at the operating wavelength of  $1.05 \mu\text{m}$ :  $\Delta R$  is as large as  $0.61 \mu\text{m}$  for  $\delta n_{core} = 0$  and decreases to  $0.21 \mu\text{m}$  for  $\delta n_{core} = -9 \times 10^{-4}$ .

##### 4.1. Effective indices

The effective indices of the fundamental and first higher order (HOM1) modes have been computed for different values of core index depression. The results are shown on Fig. 7. As expected both indices decrease when the core refractive index is reduced (higher  $|\delta n_{core}|$  values). More precisely, the fundamental mode curve has a unity slope because the effective index of the top-hat mode (at the wavelength of interest) is equal to the core index as explained in section 2.1. The HOM1 variation is almost linear with a slope close to 0.85. More importantly, the HOM1 effective index crosses the one of the fundamental space filling mode (calculated by the plane wave expansion method [24]) associated to the air-silica cladding ( $n_{FSM}$ ) around  $\delta n_{core} = -8 \times 10^{-4}$ . This value acts as a cut-off for the HOM1: the fiber core supports only the fundamental mode for  $|\delta n_{core}| > 8 \times 10^{-4}$ . Indeed, for larger  $|\delta n_{core}|$ , the HOM1 spreads very significantly into the cladding because its effective index is then smaller than the effective index of the cladding. This behavior is confirmed in the next paragraph dealing with the evolution of the confinement loss (CL) and mode effective area ( $A_{eff}$ ) versus  $\delta n_{core}$ .

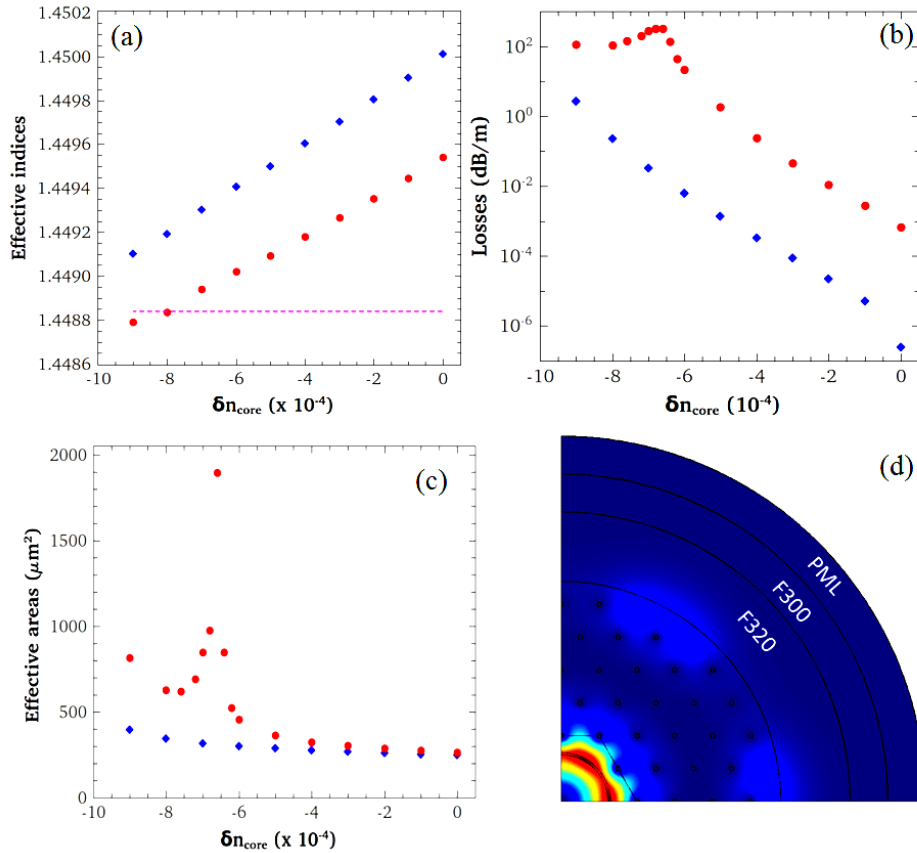


Fig. 7. (a) Effective indices for fundamental (blue diamonds) and first high order (red circles) modes. The magenta dashed line corresponds to the cladding refractive index denoted  $n_{FSM}$ . (b) Confinement losses for the fundamental (blue diamonds) and HOM1 (red circles) modes. (c) Effective areas for fundamental (blue diamonds) and HOM1 (red circles) modes. (d) Transverse intensity profile for HOM1 computed for  $\delta n_{core} = -7 \times 10^{-4}$ .

#### 4.2. Optical losses and effective areas

Figures 7(b) and 7(c) represent the variation of the CL and effective area of both modes with respect to the core index depression. In the case of the fundamental mode, both CL and effective area increase when  $\delta n_{core}$  decreases. This behavior can be simply understood by considering that larger  $|\delta n_{core}|$  leads to a decrease of the difference between the fundamental mode effective index and  $n_{FSM}$  and hence to a decrease of the mode confinement. For the same reason a similar trend is observed for the HOM1. However an extra peak is observed in the range  $-8$  to  $-6 \times 10^{-4}$  on both curves associated to this mode. This large increase of the effective area ( $> 500 \mu m^2$ ) and CL ( $> 100$  dB/m) is due to a resonant coupling with modes localised between the last air holes ring of the holey cladding and the F320 layer as illustrated on Fig. 7(d). These two curves confirm that this HOM1 can be completely disregarded for  $|\delta n_{core}| > \sim 6 \times 10^{-4}$  (any bending of the fiber will strip off this mode). These numerical results thus validate our strategy to get a single-mode fiber by using a silica core of slightly lower refractive index than the one used in the air/silica cladding. For comparison, the  $d/\Lambda$  required to get the HOM1 effective index equal to  $n_{FSM}$  (as was the case for  $\delta n_{core} = -8 \times 10^{-4}$  in Fig. 7(a)) in a structure having the same core diameter but with  $\delta n_{core} = 0$  is as low as 0.03, i.e. a value very difficult to obtain experimentally if not impossible.

Finally we can estimate that the  $\delta n_{core}$  in Fiber A is in this range of  $-8$  to  $-7 \times 10^{-4}$  as the numerical CL and effective mode area of the fundamental mode are respectively in the range 0.033 to 0.23 dB/m and 317 to 340  $\mu\text{m}^2$  i.e. values close to the experimental ones (see section 3).

## 5. Conclusion and outlooks

We report on the fabrication and characterization of an optical fiber with an improved flattened intensity profile around 1.05  $\mu\text{m}$  with single-mode behaviour. The new strategy and the fabrication procedures enabling these results are described in details. In particular the advantage of using a silica core with a slightly lower refractive index than the silica used for the microstructured cladding is demonstrated through numerical studies.

This new kind of optical fiber paves the way for a new generation of all-fiber systems able to mark or cut with a high degree of accuracy and flexibility thanks to their high spatial coherence insured by the single mode operation of the fiber. Other applications such as high harmonic generation in gases [25] and attosecond pulse generation [26, 27] could also benefit from this new design thanks to homogeneity of intensity profile. Future works will aim at increasing the fiber effective area and realizing active and polarization maintaining versions of our current design.

## Acknowledgments

We warmly acknowledge Rémi Habert for technical assistance on characterization of the fibers and Olivier Vanvincq for providing us the plane wave expansion code. This work was partly supported by French Ministry of Higher Education and Research, the Nord-Pas de Calais Regional Council and FEDER through the "Contrat de Projets Etat Région (CPER) 2007-2013" and the "Campus Intelligence Ambiante" (CIA).